

## Mechanical properties of thin hard coatings on TiC-NiMo substrates

Can Emrah Yaldiz<sup>a</sup>, Renno Veinthal<sup>b</sup>, Andre Gregor<sup>b</sup>  
and Kyriakos Georgiadis<sup>c</sup>

<sup>a</sup> Faculty of Mechanical Engineering, RWTH Aachen, Templergraben 55, 52056 Aachen, Germany; can.emrah.yaldiz@rwth-aachen.de

<sup>b</sup> Department of Materials Engineering, Tallinn University of Technology, Ehitajate tee 5, 19086 Tallinn, Estonia; {renno.veinthal, andre.gregor}@ttu.ee

<sup>c</sup> Fraunhofer Institute for Production Technology, Steinbachstr. 17, 52074 Aachen, Germany; Kyriakos.Georgiadis@ipt.fraunhofer.de

Received 3 September 2009, in revised form 7 October 2009

**Abstract.** The present study focuses on TiC-based composites with Ni-Mo binders and thin coatings (TiN, (Ti,Al)N, TiCN, nc-(Al,Ti)N/ $\alpha$ -Si<sub>3</sub>N<sub>4</sub>), produced by the Physical Vapor Deposition technique. The influence of two different Ni:Mo binder ratios (2:1 and 1:1) on the properties of the substrate and coating systems was evaluated. The effect of the substrate surface roughness on the overall substrate/coating system was also investigated. Nanocomposite nACo® coatings showed the highest hardness value. In addition, these coatings also have lower modulus values, which makes them the best candidate for wear-resistant applications. TiCN coatings have the second highest hardness value, but due to poor adhesion qualities, especially at higher roughness values, delamination was found to be present even directly after the coating process without any load. This is assumed to be related to the higher inherent residual stresses of TiCN coatings with TiC NiMo cermets.

**Key words:** TiC-NiMo cermet, PVD coating, nanoindentation, surface roughness.

### 1. INTRODUCTION

Tungsten-free TiC-NiMo cermets are very hard and have low susceptibility to diffusion and adhesion and high oxidation and wear resistance at elevated temperatures [1].

TiC-base cermets offer an attractive combination of high specific mechanical properties, such as strength/density, because of their relatively low density [2]. A general comparison of TiC-based cermets and WC-Co hardmetals reveals their

advantages and disadvantages. The coefficient of friction against steel counter body for titanium carbide-based cermets is approximately 1.5–2 times lower than that of WC-based hardmetals [3]. Moreover, maximum service temperatures for TiC are much higher and their density is 2–3 times lower. However, they exhibit lower thermal conductivity; in addition, their thermal expansion coefficient is about twice higher [4]. Finally, they show lower Young's modulus, endurance limit, thermal stability, transverse rupture strength, fracture toughness, and plasticity. Also, reprocessing of TiC-based cermets is more complicated [4,5].

Using a hard coating on machining tools in order to improve tool lifetime has become a standard application in industry. In order to realize these promised benefits, the properties of coatings and relationships between them as well as with the overall coating performance need to be understood. Figure 1 shows some of the properties of coating/substrate systems. Only after understanding these properties, coating processes can be optimized in order to produce tailor-made coatings for particular applications.

It would be very time consuming and difficult to investigate all of these parameters to characterize a coating/substrate pair. Instead, some fundamental properties were chosen to reflect the character of the coating/substrate system for a wide range of applications. Among them there are hardness and adhesion properties. The tools for testing are discussed below in detail.

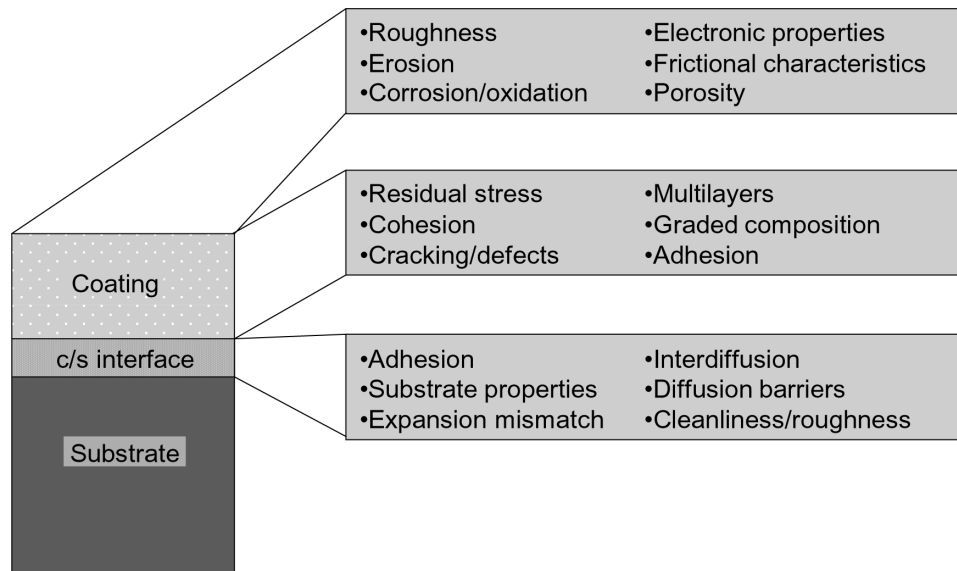


**Fig. 1.** Important coating and substrate parameters.

## 2. EXPERIMENTAL PROCEDURES

In order to compare various samples to meet the objectives of this research, first the substrates were fabricated. After fabrication of a sufficient number of substrates, they were coated with the chosen coatings. When the coating deposition was completed, the samples were analysed. Individual steps of the process are outlined below.

### 2.1. Sample production

Sample production consisted of two distinct steps: substrate fabrication and coating deposition. Two different types of substrates with varying binder content were fabricated and within each type substrate surfaces were treated to have varying degrees of roughness values.

Two different types of substrates were fabricated with the help of conventional P/M routine: TiC in nickel-molybdenum matrix, with Ni:Mo ratios of 2:1 and 1:1. The dimensions of substrate samples were  $15 \times 5 \times 25$  mm.

The pre-sintering regime was selected according to [2]. After pre-sintering, the samples were taken to the Sinter-HIP. In the Sinter-HIP process, the samples were sintered in vacuum and in a high-pressure environment, respectively. The regime consisted of various steps, including temperature increase stepwise up to  $1500^\circ\text{C}$  in vacuum, replacing vacuum with argon, pressurizing it up to 50 bar, dwell time, cool-down and depressurizing. The manufacturing technology is described elsewhere [5].

Further the specimen preparation included surface grinding to four different average roughness values, namely to  $R_a$  equal to 0.2, 0.1, 0.05 and  $0.005 \mu\text{m}$ . In every roughness category, five samples of each substrate type were prepared (in total ten per a roughness category). After sintering, every sample was first ground with the  $40 \mu\text{m}$  grinding paper. Then the samples were gradually polished to the required  $R_a$  values in the order of diamond grit sizes of 40, 20, 9, 3 and  $1 \mu\text{m}$ . The surface roughness was measured with the *Mahr* Perthometer.

### 2.2. Coating deposition

Platit  $\pi$ -80 was used as the PVD deposition system. Five different coatings: TiN, TiCN, TiAlN, AlTiN, and nc-(Al,Ti)N/ $\alpha$ - $\text{Si}_3\text{N}_4$ , ranging from monolayers to gradient coatings and nanostructured coatings, were deposited. Coating thickness was set to  $2.0 \mu\text{m}$ , and the loading factor was set to 25% in the coating program.

Before coating deposition, the substrate was prepared and cleaned in an ultrasonic bath. Arc cleaning of sample surfaces was done at  $450^\circ\text{C}$ , sample surfaces were cleaned with a pulsed Ar glow discharge. Moreover, the Ti cathode was also cleaned with Ar plasma, followed by the Ti etching process.

After the initial processes, process parameters for different coatings differed significantly. Standard Platit coating recipes were used in order to deposit the coatings. Table 1 shows the main process parameters for each coating type.

**Table 1.** Process parameters for coating deposition [6]

Coating	Bias voltage, V	Pressure, mbar	Ti/Al/AlSi cathode arc current, A	Temperature, °C	Ar/N <sub>2</sub> ; C <sub>2</sub> H <sub>2</sub> flow, sccm
TiN	-75...-120	$8 \times 10^{-3}$	(100-125)	450	6/200
TiCN	-60...-120	$(5-7) \times 10^{-3}$	(120-130)	450	6/(165-180); 7/39
TiAlN	-60...-150	$8 \times 10^{-3}-1.5 \times 10^{-2}$	(85-125)/(65-115)	475	6/200
AlTiN	-60...-150	$4 \times 10^{-3}-1.2 \times 10^{-2}$	(60-125)/(52-130)	430-450	6/(150-200)
nACo®	-75...-150	$9 \times 10^{-3}-1.2 \times 10^{-2}$	(82-125)/(65-100)	435-475	6/200

### 2.3. Coating structure and thickness

After deposition, the corresponding coating thickness was measured using the Kalo-Max Ball-Crater test method. In this method, a hard metal ball with diamond suspension is used to wear out a crater on the coated surface until the substrate is exposed. Then the resulting crater dimensions (inner and outer crater diameters) are measured under optical microscope to calculate the coating thickness  $t$ . The calculation is done using the following equation:

$$t = \sqrt{R_{\text{ball}}^2 - \left(\frac{D_i}{2}\right)^2} - \sqrt{R_{\text{ball}}^2 - \left(\frac{D_o}{2}\right)^2}. \quad (1)$$

For structure analysis the coated samples were broken into two pieces in order to obtain SEM cross-section images.

### 2.4. Indentation testing for coating adhesion

In order to test the adhesion quality of the coatings, the well-known Rockwell adhesion test method was used [7]. A Rockwell hardness-testing machine, conforming to the requirements of EN ISO 6508-2, was applied. Every sample was indented at four different representative locations as a minimum. Indentations were made in a direction perpendicular to the specimen surface. Sample surfaces were free from dust, oil, and other contaminations. A load of 598 N (60 kgf), i.e. Rockwell A scale, was used in order to conform to the relevant standards [7]. The indented samples were then analysed with an optical microscope at a magnification of 100× and results were classified into the categories given in the CEN/TS 1071-8 standards [7].

### 2.5. Nanoindentation for hardness and modulus

Nanoindentation tests for measuring hardness and modulus were conducted on a Micromaterials Nano Test platform using a standard Berkovich indenter with tip radius of 100–200 nm.

To analyse changes in hardness over coating thickness; indentations with different depths were necessary. Indentations of 1, 5, 10, 20, 30, 50, 75, 150 and 300 mN were performed on the sample. The initial load was 0.03 mN, and then the indentation load was applied as a ramp that reached the full load in 20 s. After a 10-s dwell time, the load was relieved in another 20 s. For each load, seven different locations were indented.

After the load *vs* depth data was collected, the resulting curves were first visually observed, and some problematic indents due to various extrinsic process parameters, such as external vibrations or fluctuations in the input voltage etc., were removed. Once the indentation cycle was completed and the corresponding load *vs* depth data was logged, the raw data was analysed with the Oliver Pharr power-law fitting method to determine the hardness and modulus values. Details of the Oliver Pharr power-law fitting can be found in [8].

Because some of the indentation loads were very small, their resulting indentation depths were also very low and at low depths the influence of the tip geometry of the diamond indenter on the diamond area function was included in the analysis step.

To calculate the actual diamond area function, a series of indents with loads ranging from 0.5 to 150 mN were conducted on a fused silica sample. Fused silica (quartz) has very high purity and extremely homogeneous distribution of mechanical properties; therefore it is the standard material in nanoindentation calibration tests. From the raw depth *vs* load data, the software calculates the best diamond area function in order to compensate for the diamond tip geometry for both low and high loads and indentation depths. A good fit was found for

$$A = 2393.17d + 21.61d^2, \quad (2)$$

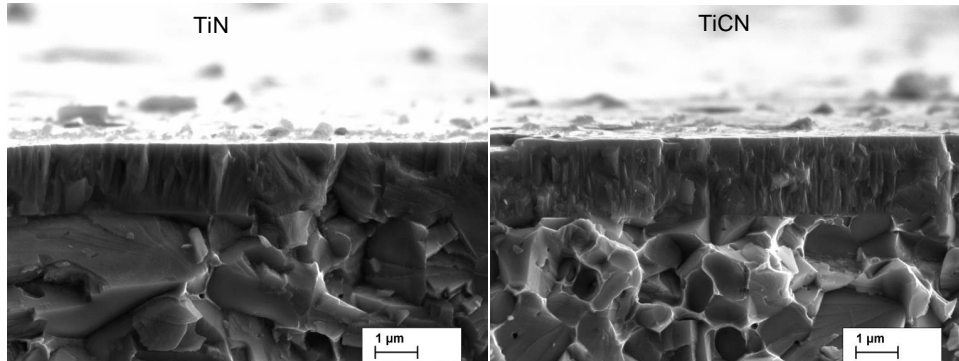
where  $d$  denotes the indentation depth and  $A$  equals the projected diamond area.

### 3. RESULTS AND DISCUSSION

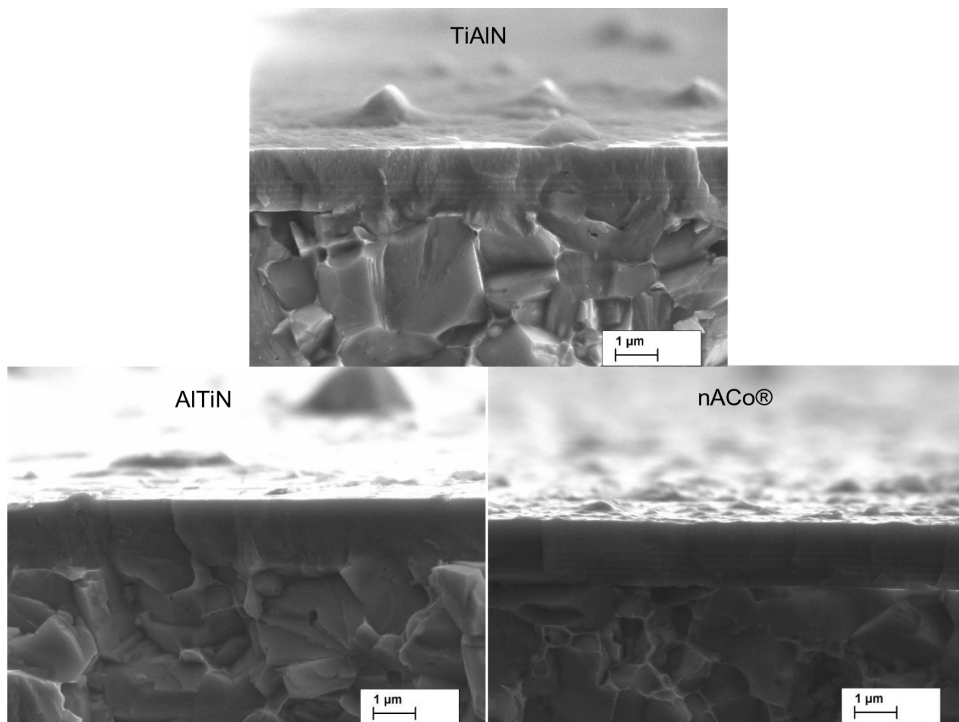
#### 3.1. Coatings structure

Figure 2 shows the SEM cross-section images of the broken samples for TiN and TiCN coatings. In both samples, a columnar microstructure is observed. Some droplet formation was also observed; however, the size of the droplets is smaller than that of the coatings with aluminium content. Coating thickness was also calculated from the pictures with an image analysis software that was found to be 1.61 and 1.85  $\mu\text{m}$  for TiN and TiCN coatings, respectively.

For coatings consisting aluminium, higher rates of droplet formation were observed. The melting temperature of aluminium is lower than that of the other components in the coating and the substrate, and because of this property, aluminium cathodes are more susceptible to droplet formation. As seen in Fig. 3,



**Fig. 2.** SEM cross-section pictures for TiN- and TiCN-coated samples.



**Fig. 3.** Cross-section pictures for TiAlN-, AlTiN- and nACo®-coated samples.

TiAlN and AlTiN coatings have droplets on the surface, with diameters close to or more than 1  $\mu\text{m}$ . The nACo® coatings also have some droplet formation on the surface, but their sizes are considerably smaller than those of TiAlN and AlTiN coatings.

TiAlN and nACo® coatings were deposited as multilayered, also verifiable from the SEM pictures (Fig. 3). In both coatings, below the alternating multilayered structure, the top layer is a gradient layer with thickness higher than that of any other layer below it. AlTiN, on the other hand, was deposited as a gradient single-layer coating.

### 3.2. Coating thickness analysis

Average results for different coating types are shown in Table 2. Coating thickness results from the ball crater test were verified with the SEM cross-section pictures and image analysis.

SEM image results are consistently about 1%–10% lower than the ball crater test results. This is related to the slightly inclined positioning of the samples on the specimen stub. If the inclination angle is  $\theta$  deg, the measured thickness is  $t_m$  and the real thickness is  $t_r$ , then the relationship between the three can be expressed as

$$t_r = t_m / \cos \theta, \quad (3)$$

which explains consistent difference between the SEM image and the ball crater test results.

### 3.3. Coating adhesion

The results of the Rockwell adhesion tests revealed a common trend between all coatings, regardless of the substrate binder ratio. For samples with fine surface topographies, such as  $R_a$  equal to 0.005 or 0.05  $\mu\text{m}$ , coating adhesion was found to be sufficient for all coating types (Class I – cracking adhesive delamination of the coating, Fig. 4, left). As the substrate surface roughness increased to  $R_a$  equal to 0.1 or 0.2  $\mu\text{m}$ , coating adhesion quality dropped to poor levels and showed full delamination around the indent (Class III – complete adhesive delamination, Fig. 4, right).

**Table 2.** Average coating thickness of different coating types

Coating type	Average thickness, $\mu\text{m}$	
	Ball crater test	SEM
AlTiN	1.75	1.61
TiCN	1.98	1.85
TiAlN	1.68	1.51
TiN	1.71	1.62
nACo®	1.51	1.49

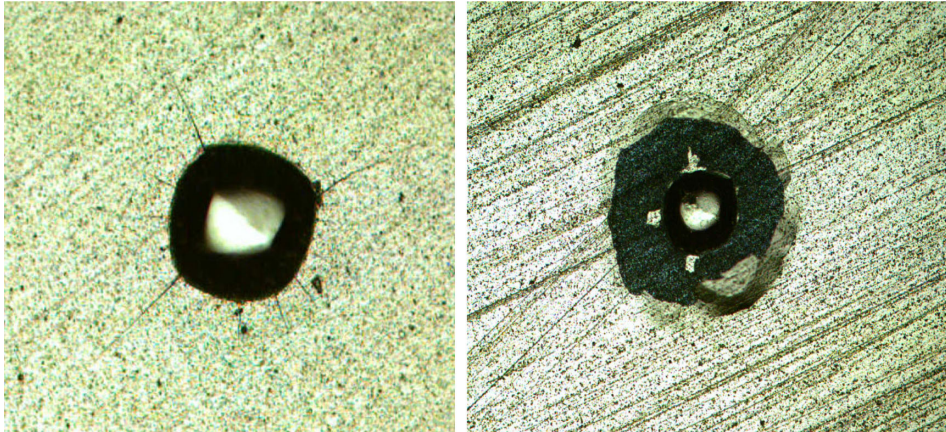


**Fig. 4.** Class I (left) and Class III (right) indentation marks on TiN samples.

### 3.4. Nanoindentation for hardness and modulus measurements

After the function  $A(d)$  was found, the indentation data was analysed following the Oliver and Pharr method [8], and the mechanical properties were calculated. The resulting hardness values at different depths (as a percentage of the coating thickness) are shown in Fig. 5.

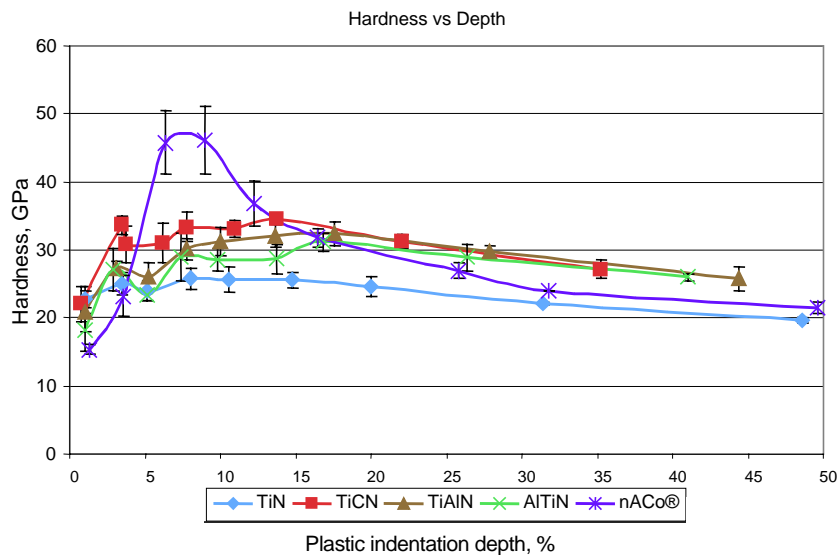


**Fig. 5.** Hardness dependence on the plastic indentation depth.

Figure 5 demonstrates that at low load ranges 1–5 mN, corresponding to plastic indentation depths up to 3% of the total coating thickness, the results are consistently lower than at higher loads. The reason of this lower hardness value is attributed to the fact that no further polishing was done on the coated samples, and the effects of the roughness profile were very pronounced at the lower load regions. Depending on the part of the roughness profile the indenter hits a particular value (i.e. peak, valley or in-between), usually the results tend to be lower than the actual values. With the increasing load, the effects of the roughness profile diminish due to the increased indenter depth, and the hardness values increase. After passing 10% of the thickness limit as the plastic indentation depth, the influence of the substrate starts to affect hardness measurements, and hardness starts dropping.

As a rule of thumb for healthy hardness measurements, the plastic indentation depth should not be higher than 10% of the coating thickness in order to avoid the influence of the relatively softer substrate. As shown in Fig. 5, the very low load region is also affecting the overall result due to the roughness profile. Therefore, to quantify the core hardness of the coatings, measurements with 20 mN were chosen as the most suitable ones. Because the resulting indent is deep enough to be free from the influence of the roughness profile, but still below the 10% coating thickness depth, influence of the substrate is eliminated. Table 3 shows the hardness and modulus measurement results.

#### 4. CONCLUSIONS

The **coating thickness** measurements revealed that coating thickness was slightly below the set value of 2.0  $\mu\text{m}$ , which was due to the selected loading factor of 25%. Coating thickness values were consistent and even among the measured samples.

**Nanoindentation** results from the 1 and 5 mN hardness measurements were lower than expected due to the surface roughness effects, more pronounced at low indentation loads. Polished samples should be used for measurement in order to minimize the effects of the roughness profile and to increase the accuracy of core hardness measurements.

Concerning **core hardness measurements**, nACo® coatings showed the highest hardness value. These coatings also have a lower modulus value, which

**Table 3.** Nanoindentation results

Coating type	Hardness, GPa	Modulus, GPa	H/E
TiN	25.86±1.55	357±21.4	0.072
TiCN	31.04±2.82	345±31.3	0.090
TiAlN	30.17±1.52	342±17.2	0.088
AlTiN	29.00±3.51	325±39.3	0.089
nACo®	46.18±4.95	320±34.3	0.144

makes them the best candidate for wear resistant applications. The TiCN coatings have the second highest hardness value, but they exhibited poor adhesion qualities, especially with higher roughness values, as delamination was present even directly after the coating process without any load. This is assumed to be related to the higher inherent residual stresses of TiCN coatings with TiC-NiMo cermets. Further research should be conducted in order to analyse and optimize the adhesion properties of this type of coating-substrate pairs.

According to the **Rockwell Adhesion Testing**, coatings on substrates with surface roughness 0.05 and 0.005  $\mu\text{m}$  show good adhesion characteristics. However, with increasing substrate roughness values, adhesion drops dramatically and therefore should be controlled carefully in design and manufacturing of the tools to be coated.

### ACKNOWLEDGEMENTS

Dr. Marcus Morstein from Platit AG is acknowledged for his advice. This work was supported by the Estonian Ministry of Education and Research (target financed project SF01400091) and the Estonian Science Foundation (grant No. 7227).

### REFERENCES

1. Kübarsepp, J., Klaasen, H. and Pirso, J. Behaviour of TiC-base cermets in different wear conditions. *Wear*, 2001, **249**, 229–235.
2. Kübarsepp, J., Pirso, J. and Klaasen, H. Tribological characterization of TiC-base cermets. In *Proc. 2000 Powder Metallurgy World Congress*. Kyoto, 2000, Part 2, 1633–1636.
3. Pirso, J., Viljus, M. and Letunoviš, S. Friction and dry sliding wear behaviour of cermets. *Wear*, 2006, **260**, 815–824.
4. Ellis, J. L. and Goetzel, C. G. *ASM Handbook*, Vol. 2, Properties and Selection: Nonferrous Alloys and Special-Purpose Materials, 1991, ASM.
5. Juhani, K. *Reactive Sintered Chromium and Titanium Carbide-Based Cermets*. PhD Thesis, TUT Press, 2009.
6. Platit Technical Specifications: [www.platit.com](http://www.platit.com)
7. Technical Specification Guide CEN/TS 1071-8:2004 of the European Committee for Standardization, “Advanced technical ceramics – Methods of test for ceramic coatings, Part 8: Rockwell indentation test for evaluation of adhesion”.
8. Oliver, W. C. and Pharr, G. M. Measurement of hardness and elastic modulus by instrumented indentation: Advances in understanding and refinements to methodology. *J. Mater. Res.*, 2004, **19**, 3–20.

## **Õhukeste kõvapinnete mehaanilised omadused TiC-NiMo-kermistest alusel**

Can Emrah Yaldiz, Renno Veinthal, Andre Gregor ja Kyriakos Georgiadis

On käsitletud füüsikalise aurustamise (PVD) meetodil saadud õhukeste kõvapinneteid (TiN, (Ti,Al)N, TiCN, nc-(Al,Ti)N/ $\alpha$ -Si<sub>3</sub>N<sub>4</sub>) nikkel-molibdeen-(Ni-Mo) sideainega titaankarbiid- (TiC) kermistest. On uuritud sideaine Ni:Mo suhte (2:1 ja 1:1) mõju aluse ning pinde mehaanilistele omadustele. On vaadeldud ka substraadi pinnakareduse mõju süsteemile alusmaterjal-pinne tervikuna.

Nanokomposiitsed nACo®-pinnetel on suurima kõvadusega. Lisaks iseloomustab neid pindeid väiksem elastsusmoodul, mistõttu sobivad need vaadeldud pinnetest kõige paremini kulumiskindlust nõudvatesse rakendustesse. Kõvaduselt järgmise, TiCN-pinde puuduseks on ebapiisav adhesioon alusmaterjaliga (seda eriti suurema pinnakareduse juures), mistõttu esineb pinde ja alusmaterjali vahelist kihistumist (delaminatsiooni) isegi vahetult pärast pindamisoperatsiooni lõppu. See on seletatav kõrgete pinnapingete tekkimisega TiCN-pinde ja TiC-NiMo-süsteemis. Edasine uurimistöö peaks keskenduma vaadeldavate pinnete ja alusmaterjalide adhesiooni analüüsile ning parandamisele.